Photorefractive *p-i-n* diode quantum well spatial light modulators

I. Lahiri,[a] K. M. Kwolek, and D. D. Nolte
Department of Physics and the MRSEC for Technology-Enabling Heterostructure Materials, Purdue University, West Lafayette, Indiana 47907-1396

M. R. Melloch
School of Electrical Engineering and the MRSEC for Technology-Enabling Heterostructure Materials, Purdue University, West Lafayette, Indiana 47907-1285

(Received 9 March 1995; accepted for publication 26 June 1995)

We demonstrate the performance of all-semiconductor photorefractive *p-i-n* diodes operating in the longitudinal quantum-confined Stark geometry. Low-temperature-grown shallow quantum wells provide high-mobility vertical transport, and potential steps incorporated into the semiconductor buffer layers increase the transit time across the buffer and therefore increase the quantum efficiency for trapping of charge before it is swept out to the doped *p*-type and *n*-type contacts. The buffer design and the doped contacts both make all-semiconductor photorefractive devices possible, with peak transient output diffraction efficiencies approaching 3%, but without the need for dielectric insulating layers. We also redefine device speed by making a distinction between transient rise times and frequency response, showing that in these *p-i-n* devices the update rate is an order of magnitude slower than the inverse rise time. © *1995 American Institute of Physics.*

Photorefractive quantum wells and thin films[1–3] are dynamic holographic materials that combine the advantages of large excitonic electroabsorption with large carrier mobilities to produce high-sensitivity[4] holographic devices that are compatible with many image processing applications. The design of appropriate buffer layers has been one of the key features of photorefractive longitudinal-field design and performance,[5] as in earlier device structures that used free-carrier screening in nonpixellated quantum well devices.[6,7] Optimum performance of photorefractive devices has previously relied upon nonsemiconductor insulating buffers of SiO_2 or SiN to prevent charge transport to the contacts and to eliminate leakage currents in the broad-area devices.[8]

In this letter, we present the performance of longitudinal-field photorefractive *p-i-n* diode designs using all-semiconductor trapping buffers and doped contacts. The doped *n*-type and *p*-type contacts had been proposed[9,10] to replace semitransparent contacts used in some previous designs,[5,11] and to give the device low-leakage currents when the device is reverse-biased during operation. The buffer layers are composed of low-temperature-growth (LTG) AlGaAs.[12] The LTG materials have ultrafast lifetimes that extend down to picoseconds,[13] which therefore produce spatial resolutions down to 1 μm in transverse-field geometries,[2] and down to approximately 10 μm in longitudinal-field geometries.[8,14] To ensure that all carriers that are injected into the buffer from the electro-optic layer are trapped, we have incorporated potential steps into the buffer that increase the transit time of the carriers, giving them time to trap at defects.

In our experiments, we distinguish between transient-time response (TTR) and Fourier-time response (FTR) measurements of the diffraction efficiency. The TTR is obtained by recording the diffraction as a function of time in a digital storage oscilloscope. The peak transient signal is the largest diffracted intensity after the application of the electric field to the device. The FTR signal is obtained using lock-in detection, referenced to the frequency of the repetitive applied voltage. The Fourier diffraction efficiency is proportional to the first Fourier-time coefficient of the diffracted signal and is related to the time-integrated response of the diffracted signal. The distinction between TTR and FTR is important, because the diffraction signal typically has a large and rapid diffracted signal spike shortly after the voltage is applied, but which quickly decays. For image processing applications, the time-integrated diffracted signal is the most important value because it describes the average number of photons per second arriving at focal planes or charged coupled device (CCD) arrays. An additional important issue for device performance in imaging applications is the fastest allowable repetition rate between pulses that defines the frame rate of the device. We show in our tests that the optimum repetition rate for ac fields applied to the devices is considerably slower than the inverse rise time, which requires a reassessment of the definitions of the speed of the longitudinal-field geometries.

Two designs were tested and had relatively similar performance in our experiments. The first device had multiple quantum wells (MQWs) grown at standard temperatures and which were subsequently proton implanted, while the second device used quantum wells grown at low-substrate temperatures.[15] Both devices were grown by molecular beam epitaxy (MBE) and used LTG buffer layers that also incorporated potential steps to retard the transit time of the carriers to the contacts.

Device 1 had a MQW layer grown at standard temperatures that consisted of 110 periods of $Al_{0.3}Ga_{0.7}As/GaAs$ quantum wells with 10 nm wells and 3.5 nm barriers. The wells were grown using an As_2 to Ga beam equivalent pressure ratio of 15. The buffers were symmetric and consisted of LTG $Al_{0.2}Ga_{0.8}As$ 700 nm thick, followed by a 200 nm of LTG $Al_{0.3}Ga_{0.7}As$. The LTG layers were grown at a substrate temperature of 280 °C, all other layers were grown at 600 °C. The potential step provides the carriers time to trap

[a]Electronic mail: lahiri@physics.purdue.edu

 0003-6951/95/67(10)/1408/3/$6.00

in the LTG AlGaAs and effectively replaces the nonsemiconductor insulating layer in previous longitudinal-field designs. A 50 nm spacer of standard-temperature-growth $Al_{0.3}Ga_{0.7}As$ was placed between the doped contacts and the buffer layer.

Device 2 used an As_4 to Ga beam equivalent pressure ratio of 20. The structures were LTG MBE $Al_{0.16}Ga_{0.84}As/Al_{0.1}Ga_{0.9}As$ MQWs grown at n^+ GaAs substrates. Contact and stop-etch layers of *n*-type materials were grown on the n^+ GaAs substrate at 600 °C. This was followed by a LTG (320 °C) MQW layer consisting of a 100 periods of 10 nm $Al_{0.1}Ga_{0.9}As$ wells and 10 nm $Al_{0.16}Ga_{0.84}As$ barriers. The LTG superlattice was sandwiched between a step-graded buffer which consisted of 500 nm of $Al_{0.15}Ga_{0.85}As$ and 200 nm of $Al_{0.3}Ga_{0.7}As$. The LTG (320 °C) results in approximately 0.2% excess arsenic in the MQW. A 200 nm p-$Al_{0.3}Ga_{0.7}As$ (1×10^{18} cm^{-3}) layer followed by a 100 nm top p-GaAs (1×10^{19} cm^{-3}) was grown at 450 °C on top of the LTG layers. The 450 °C growth temperature for the *p*-doped layers acts as a weak *in situ* anneal of the previously grown LTG layers and results in the formation of As precipitates in the MQW region.[12,16] Details of fabrication can be found elsewhere.[15]

We performed degenerate four-wave mixing on the two device structures by writing a grating using a cw Ti:sapphire laser tuned at 850 and 790 nm for the two devices. The transmitted zero-order and the diffracted first-order signals were detected using silicon photodiodes with 650 nm long pass filters. TTR and FTR output diffraction efficiencies were measured. The electric field was modulated using a single-sided square pulse at a repetition rate of 100 Hz. The diffracted and the transmitted signals were detected using a lock-in amplifier modulated by the electric field and a mechanical chopper, respectively. All diffraction efficiencies quoted in this letter are output diffraction efficiencies, defined as the ratio of the diffracted intensity to the transmitted intensity.

Figure 1 shows the dependence of the output diffraction efficiency as a function of the applied voltage to the sample using a single-sided square pulse with a repetition rate of 100 Hz. Both TTR and FTR output diffraction efficiencies are shown. For low fields the output diffraction efficiency follows a fourth-order power law with increasing electric field. The transient output diffraction efficiency approaches 3%, an order of magnitude greater than the FTR value. However, higher intensities than shown here have produced higher device speeds and generated output diffraction efficiencies in excess of 10%. The fourth-power dependence at low fields is due to the quadratic dependence of diffraction on index and absorption gratings, which themselves depend quadratically on electric field.[3] The deviation from fourth-power dependence at the higher electric fields may be caused by several mechanisms: lateral drift that reduces the electric field modulation in the quantum wells,[17] reduced quantum efficiency for carrier trapping in the buffers at higher fields, and deviation of the electroabsorption from quadratic dependence on field. Because we use only semiconductor buffers, the carriers can overcome the moderate potential barrier that separates the buffer layers from the contacts. At higher fields, the electrons have higher ballistic velocities, which enable them to overcome the barrier more effectively, preventing sufficient time to trap the charge.

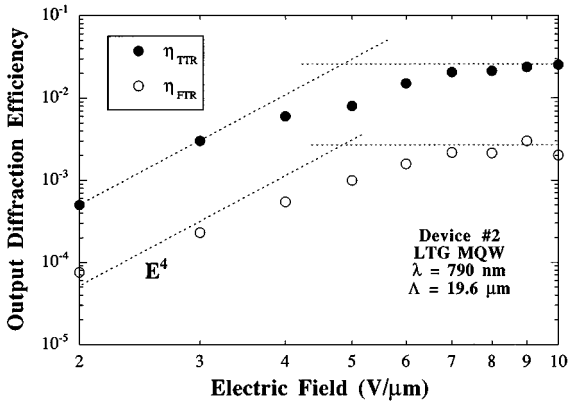

FIG. 1. Output diffraction efficiency for TTR and FTR in response to a square-wave reverse-bias voltage on device 2 with LTG quantum wells. Both responses vary approximately with fourth power on electric field for small fields but saturate for fields larger than 50 kV/cm. The TTR is consistently an order of magnitude larger than the FTR.

The frequency dependences of the FTR of both devices are shown in Fig. 2 for square-wave and sinusoidal reverse-bias fields, at a fringe spacing of 20 μm with an intensity of $\approx$10 mW/cm^2. The device with quantum wells grown at normal growth temperatures has a higher Fourier diffraction efficiency and higher frequency response. This behavior is consistent with smaller defect densities in device 1 from proton implantation relative to the high-defect densities in the LTG quantum well layer in device 2.[11] Shorter lifetimes of the photocarriers in the LTG materials slow down the dielectric relaxation rate. Carrier lifetimes in the LTG quantum wells are approximately 15 ps,[15] while the proton-implanted quantum wells have lifetimes of approximately 200 ps.[18] Therefore the LTG response rate is expected to be approximately an order of magnitude slower than for the proton-implanted device. This expectation is borne out by the data. It is important to note that the difference in trap densities in the MQW layer primarily controls the saturation intensity I_{sat} for which the photoconductivity exceeds the dark conductivity, leaving other aspects of device performance unaffected.

Also shown in Fig. 2 is the difference between square-wave and sine-wave applied fields. The square-wave dependence produces higher FTR diffraction efficiencies (as well as transient diffraction signals). This higher response is related to the formation dynamics of the trapped space charge that screens the applied fields. The large transient diffraction efficiencies are generated by the relatively fast initial screening of the applied fields in the bright fringes, followed by lateral drift and diffusion that reduces the spatial field modulation in the quantum wells. The solid lines in Fig. 2 are fit to the equation of the equivalent circuit for the longitudinal geometry presented in Ref. 3. The *RC* time constants for these devices at this intensity are 300 μs for device 1 and 3 ms for device 2. These numbers are again consistent with the difference in defect densities between the proton-implanted MQW device and the LTG MQW device. It is important to

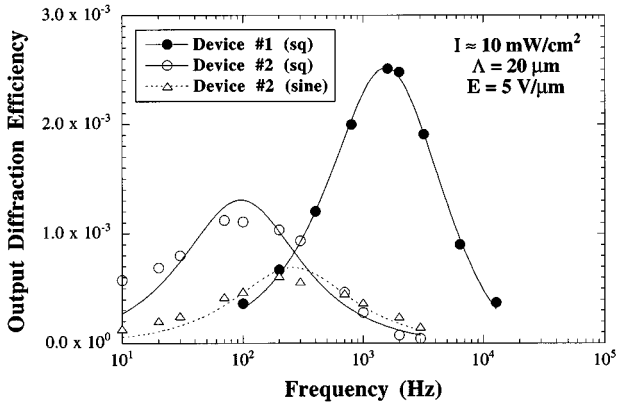

FIG. 2. Fourier response output diffraction efficiency as a function of frequency for both device designs. The proton-implanted device operates at an order of magnitude larger frequency than the device with LTG quantum wells for the 10 mW/cm^2 illumination. Response to a square wave for device 2 is significantly larger than for a sine wave.

point out that the rise times of the transient diffraction response in these devices is considerably shorter than the *RC* time constant fits from Fig. 2. Rise times of 50 μs are observed in the transient response for our intensities and defect densities. It is important to note that both the rise time and the resonant frequency are linear functions of incident intensity. Therefore, the ratio of the optimum repetition rate to the inverse rise time is intensity independent and is approximately equal to 0.1. Because the intensity-dependent repetition rate defines the frame rate of the device, this should be the relevant device speed, rather than relating device speed to rise time.

To further study the temporal response and differences between pulsed operation and repetitive operation, in Fig. 3 we show the dependence of the TTR and FTR on pulse duration for a fixed repetition time of 10 ms for device 2. The pulsewidth was varied from 192 μs to 9.2 ms. The TTR output diffraction efficiency is relatively independent of the width of the pulse for pulse widths longer than 600 μs. These

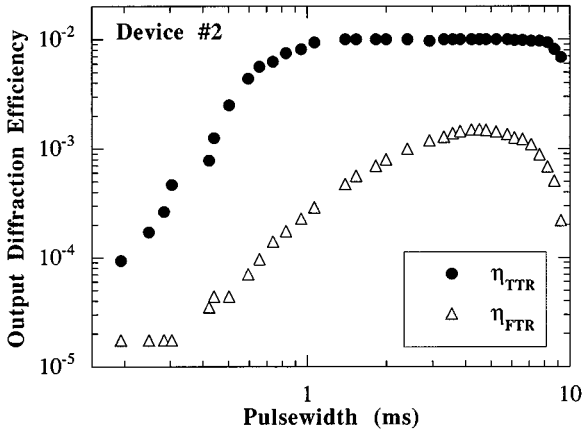

FIG. 3. TTR and FTR output diffraction efficiencies as functions of the pulsewidth of the modulating electric field. Experimental data for the output diffraction efficiency were taken at a fringe spacing of 20 μm with an incident laser intensity of 5.0 mW/cm^2 at $\lambda = 790$ nm. The electric field was modulated using a single-sided pulse of 5 V/μm at a repetition rate of 100 Hz.

results further suggest that the relevant speed for image processing applications with photorefractive quantum wells in the longitudinal-field geometry is controlled by the repetition rate and duty cycle and not by the rise time of the transient signal. The maximum repetition rate at a given intensity is likely to be limited by the charge relaxation in the buffer layers. If the voltage is repeated too rapidly for that intensity, there is insufficient time for the charge to relax.

In our study of the photorefractive *p-i-n* quantum well diode structures, we have observed consistent good photorefractive performance using the two different buffer designs. Both of the designs incorporate potential steps that retard the transit time of carriers across the buffer, allowing time for the carriers to trap at defects. These buffer designs are combined with *p*-type and *n*-type doped contacts that help reduce leakage currents when the devices are operated under reverse bias. Together, these design features make it possible to fabricate and operate all-semiconductor longitudinal-field devices. It is especially important to note that these designs require almost no postprocessing of the semiconductor growth, significantly improving the ease of device fabrication.

This work was supported in part by the NSF under Award Nos. ECS-9414800 and DMR-9400415. D. D. Nolte also acknowledges support by the NSF PYI program. M. R. Melloch acknowledges support from the US Air Force Office of Scientific Research under Grant No. F49620-91-1-0031.

[1] D. D. Nolte, D. H. Olson, G. E. Doran, W. H. Knox, and A. M. Glass, J. Opt. Soc. Am. B **7**, 2217 (1990).
[2] D. D. Nolte, M. R. Melloch, J. M. Woodall, and S. E. Ralph, Appl. Phys. Lett. **61**, 3098 (1992).
[3] D. D. Nolte and M. R. Melloch, in *Photorefractive Effects and Materials*, edited by D. D. Nolte (Kluwer, Dordrecht, 1995), Chap. 7.
[4] Q. N. Wang, R. M. Brubaker, D. D. Nolte, and M. R. Melloch, J. Opt. Soc. Am. B **9**, 1626 (1992).
[5] A. Partovi, A. M. Glass, D. H. Olson, G. J. Zydzik, K. T. Short, R. D. Feldman, and R. F. Austin, Appl. Phys. Lett. **59**, 1832 (1991).
[6] Y. Kan, K. Obata, M. Yamanishi, Y. Funahashi, Y. Sakata, Y. Yamaoka, and I. Suemune, Jpn. J. Appl. Phys. **28**, L1585 (1989).
[7] K. Obata, M. Yamanishi, Y. Yamaoka, Y. Kan, J. Hayashi, and I. Suemune, Appl. Phys. Lett. **57**, 419 (1990).
[8] C. S. Kyono, K. Ikossi-Anatasiou, W. S. Rabinovich, S. R. Bowman, and D. S. Katzer, Appl. Phys. Lett. **64**, 2244 (1994).
[9] N. T. Pelekanos, B. Deveaud, C. Guillemot, J. M. Gerard, P. Gravey, B. Lambert, A. Le Corre, and J. E. Vaillet, Opt. Mater. **4**, 348 (1995).
[10] A. Partovi, Opt. Mater. **4**, 330 (1995).
[11] W. S. Rabinovich, S. R. Bowman, D. S. Katzer, and C. S. Kyono, Appl. Phys. Lett. **66**, 1044 (1995).
[12] M. R. Melloch, N. Otsuka, K. Mahalingam, C. L. Chang, J. M. Woodall, G. D. Pettit, P. D. Kirchner, F. Cardone, A. C. Warren, and D. D. Nolte, J. Appl. Phys. **72**, 3509 (1992).
[13] E. S. Harmon, M. R. Melloch, J. M. Woodall, D. D. Nolte, N. Otsuka, and C. L. Chang, Appl. Phys. Lett. **63**, 2248 (1993).
[14] P. Tayebati, K. Krishnaswami, D. D. Nolte, and M. R. Melloch, Proceedings of the 5th Top. Conf. Photoref. Mat. Eff. Dev., Opt. Soc. Am. 1995, p. 536.
[15] I. Lahiri, D. D. Nolte, E. S. Harmon, M. R. Melloch, and J. M. Woodall, Appl. Phys. Lett. **66**, 2519 (1995).
[16] M. R. Melloch, N. Otsuka, J. M. Woodall, A. C. Warren, and J. L. Freeouf, Appl. Phys. Lett. **57**, 1531 (1990).
[17] D. D. Nolte, Opt. Commun. **92**, 199 (1992).
[18] Y. Silverberg, P. W. Smith, D. A. B. Miller, B. Tell. A. C. Gossard, and W. Wiegmann, Appl. Phys. Lett. **46**, 701 (1985).